

Nonequilibrium shock-heated nitrogen flows using a rovibrational state-to-state method

M. Panesi

University of Illinois at Urbana-Champaign, Urbana, 104 S. Wright street, Champaign, Illinois 61801, USA

A. Munafò and T. E. Magin

von Karman Institute for Fluid Dynamics, chaussée de Waterloo 72, 1640 Rhode-Saint-Genèse, Belgium

R. L. Jaffe

NASA Ames Research Center, Moffett Field, Mountain View, California 94035, USA

(Received 7 March 2014; published 14 July 2014)

A rovibrational collisional model is developed to study the internal energy excitation and dissociation processes behind a strong shock wave in a nitrogen flow. The reaction rate coefficients are obtained from the *ab initio* database of the NASA Ames Research Center. The master equation is coupled with a one-dimensional flow solver to study the nonequilibrium phenomena encountered in the gas during a hyperbolic reentry into Earth's atmosphere. The analysis of the populations of the rovibrational levels demonstrates how rotational and vibrational relaxation proceed at the same rate. This contrasts with the common misconception that translational and rotational relaxation occur concurrently. A significant part of the relaxation process occurs in non-quasi-steady-state conditions. Exchange processes are found to have a significant impact on the relaxation of the gas, while predissociation has a negligible effect. The results obtained by means of the full rovibrational collisional model are used to assess the validity of reduced order models (vibrational collisional and multitemperature) which are based on the same kinetic database. It is found that thermalization and dissociation are drastically overestimated by the reduced order models. The reasons of the failure differ in the two cases. In the vibrational collisional model the overestimation of the dissociation is a consequence of the assumption of equilibrium between the rotational energy and the translational energy. The multitemperature model fails to predict the correct thermochemical relaxation due to the failure of the quasi-steady-state assumption, used to derive the phenomenological rate coefficient for dissociation.

DOI: [10.1103/PhysRevE.90.013009](https://doi.org/10.1103/PhysRevE.90.013009)

PACS number(s): 47.70.Nd, 34.50.Ez, 34.50.Lf, 34.80.Gs

I. INTRODUCTION

Modeling of the aerothermal environment encountered in hypersonic flight is characterized by a wealth of physical processes, strongly coupled to each other [1]. Strong shock waves, formed in front of the vehicles, heat up the flow, thus converting the flow kinetic energy into thermal energy. As a consequence, chemical transformations in the composition of the gas occur, and the gas becomes chemically reactive. Often, since the characteristic time of the chemical processes and the flow characteristic time are comparable, the state of the gas is out of local thermodynamic equilibrium.

In the hypersonic flight regimes, the chemical transformation occurring in the gas can drastically influence the dynamics of the flow [2]. Traditionally, the modeling of nonequilibrium effects relies on the numerical solution of a set of conservation equations, which include the following: the continuity equations for each chemical component in the gas, the set of Navier-Stokes equations, and an additional set of energy conservation equations for the description of the thermal relaxation processes of the atoms and molecules [3,4]. A self-consistent derivation of these systems of equations can be obtained by using perturbative methods [5–13]. For example, Nagnibeda and Kustova [8] adopted this method to derive a model which accurately describes the vibrational relaxation of the gas, including the effects of the relaxation on chemistry, thermodynamics, and transport properties.

These approaches rely on the correct scaling the Boltzmann equation, based on sound assumptions concerning the

characteristic time of the different relaxation processes. Thus, the assessment of the validity of the underlying assumptions is seen as a fundamental prerequisite to the mathematical derivation of the governing equations.

Today's paradigm for the aerospace science and plasma physics communities [14–20] consists of avoiding empiricism by integrating quantum chemistry databases into computational models and constructing models based on *ab initio* theories. The present work is at the interface between computational chemistry and computational fluid dynamics and aims at the development of reduced models based on microscopic theory and applying them to the macroscopic scale. The availability of *ab initio* rate parameters for elementary collisional processes has enabled the development of state-to-state (STS) models [19,21–32]. These models allow for the detailed study of kinetic processes under strong nonequilibrium conditions, for which the distribution of the internal energy levels strongly departs from the equilibrium Maxwell-Boltzmann distribution.

The most detailed models developed in the literature are rovibrational collisional models [33]. In these models the population of the internal levels is explicitly computed as a solution to the master equation governing the populations of each individual internal level. Examples of rovibrational collisional models found in literature are often restricted to computationally more tractable systems, e.g., hydrogen dissociation [34–36]. The present work aims at assessing the validity of some fundamental assumptions, often made in the modeling of high-temperature reacting flows, by using a model

free of empiricism. In the past vibrational collisional models have been widely selected as the preferred tool to accomplish this task [21,25,31,37–45]; however, these models rely on the assumption of thermal equilibrium between the translational and rotational energy modes, which is questionable [46–50] for strong nonequilibrium conditions often encountered in hyperbolic atmospheric entry applications.

Recently, state-to-state (or collisional) models have become increasingly popular, due to the availability of ever-increasing computational resources. However, multitemperature models (MT) are still the method of choice when describing the nonequilibrium effects in hypersonic flows. Multitemperature collisional models have been used extensively in the literature so far, mostly because they are easy to implement in multidimensional flow codes and they are computationally efficient given the reduced number of equations in the model.

In MT models, the physicochemical properties of the airflow are obtained through the shock layer by assuming that, for all species, the population of each internal (rotational, vibrational, or electronic) energy mode follows a Maxwell-Boltzmann distribution at its own temperature. To calculate these temperatures and the energy exchanged between all the energy modes (i.e., translational, rotational, vibrational, and electronic), conservation equations for the internal energy modes in thermal nonequilibrium are added to the conventional equations for total mass, momentum, and energy conservation. For the chemical kinetics model, macroscopic rate coefficients are assumed to depend on an empirical temperature that is a function of the different temperatures in the flow.

We study the rovibrational energy excitation and dissociation processes in nitrogen gas, behind a strong shock. In the free stream, cold nitrogen molecules at room temperature, seeded with a small amount of nitrogen atoms, are suddenly heated by several thousand degrees kelvin, driving the gas toward a strong nonequilibrium condition. The present investigation is devoted to the in-depth study of the relaxation of $N_2(^1\Sigma_g^+)$ by collision with $N(^4S_u)$. Our proposed model relies on state-specific reaction rate coefficients from the *ab initio* database developed at NASA Ames Research Center. The published results will serve as a benchmark for validation of more approximate theories [37,38,51–54] and reduced order models. Furthermore, the insights gained by the analysis of nitrogen dissociation will serve as guidelines for the development of reduced models. First steps in this direction have already been published by our group [16–18,55,56].

The paper is organized as follows: The physical model is discussed in Sec. II. In particular, the NASA Ames database is discussed in Sec. II A; the governing equations for the rovibrational, vibrational, and multitemperature collisional models are discussed in Sec. II B. Section III presents the results of the investigation and it is divided into three subsections: Section III A discusses the results obtained with the rovibrational collisional (RVC) model, starting from the analysis of the macroscopic thermodynamic parameters, down to the details of the nonequilibrium rovibrational distribution function. Section III B compares the results obtained with the different nonequilibrium reduced order models. The reasons of the discrepancies among the three models are discussed in Sec. III C.

II. PHYSICAL MODEL

A. NASA Ames database

The NASA Ames database [57–61] comprises a set of consistent thermodynamic and kinetic data for the rovibrational excitation, dissociation and predissociation of the N_2 molecule colliding with an N atom. Both chemical components are in their electronic ground state [i.e., $N_2(^1\Sigma_g^+)$ - $N(^4S_u)$ system]. While the analysis carried out in this work is restricted to the study of N_2 -N interactions, an ongoing effort addresses the study of dynamics of the $N_2(^1\Sigma_g^+)$ - $N_2(^1\Sigma_g^+)$ system [62].

The number of rovibrational energy levels $N_2(v, J)$ of the electronic ground-state of N_2 is 9390, and the indices v and J stand for the vibrational and rotational quantum numbers, respectively. The energy of the rovibrational level (v, J) can be written as the sum of the vibrational and rotational contributions as follows:

$$E_{vJ} = \tilde{E}_v + \Delta\tilde{E}_v(J), \quad v \in \mathcal{V}, \quad J \in \mathcal{J}_v, \quad (1)$$

where $\mathcal{V} = \{0, \dots, v_{\max}\}$ is the set of vibrational quantum numbers and $\mathcal{J}_v = \{0, \dots, J_{\max}(v)\}$ is the set of rotational quantum numbers for a given vibrational quantum state v . The vibrational energy \tilde{E}_v is defined as the energy of the rotationless level ($J = 0$) having vibrational quantum number v . The rotational energy is defined based on the vibrational energy as $\Delta\tilde{E}_v(J) = E_{vJ} - \tilde{E}_v$. The energy splitting adopted in Eq. (1) is arbitrary defined and other choices are possible [63]. The degeneracy of the rovibrational energy level (v, J) is as follows:

$$g_{vJ} = (2J + 1) g_{vJ}^{\text{NS}}, \quad (2)$$

$$g_{vJ}^{\text{NS}} = \begin{cases} 6 & \text{even } J \\ 3 & \text{odd } J \end{cases}, \quad v \in \mathcal{V}, \quad J \in \mathcal{J}_v.$$

The quantity g_{vJ}^{NS} is the nuclear spin degeneracy of N_2 . Its dependence on the rotational quantum number J is due to the fact that the total wave function of N_2 must be symmetric with respect to exchanging the nuclei (Bose-Einstein statistics) [57–61]. The number of vibrational energy levels is 61 ($v_{\max} = 60$) and for the vibrational ground state ($v = 0$) the maximum rotational quantum number is 279. Most of the rovibrational levels (7421) are bound (B). This means that their energy is lower than the dissociation energy relative to the $(v = 0, J = 0)$ level, equal to 9.75 eV. The remaining levels are predissociated (P), or quasibound. Thus, their energy is higher than the dissociation energy relative to the level $(v = 0, J = 0)$ but lower than the J -dependent centrifugal barrier [63]. This means they have a finite lifetime and spontaneously dissociate by tunneling through the centrifugal barrier. The numerical values of the rovibrational energy levels have been obtained by applying the Wentzel-Kramers-Brillouin (WKB) approximation [64] using the potential for N_2 developed by Leroy *et al.* [65].

The rovibrational energy levels can be also represented by sorting them by increasing energy and denoting them by means of a global index i . The correspondence between the i and (v, J) notations can be expressed as

$$i = i(v, J), \quad v \in \mathcal{V}, \quad J \in \mathcal{J}_v, \quad (3)$$

and conversely by the relations

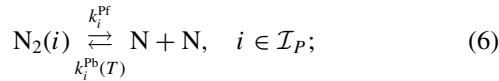
$$v = v(i), \quad J = J(i), \quad i \in \mathcal{I}_{BP}, \quad (4)$$

where \mathcal{I}_{BP} is the set containing the rovibrational levels. For the sake of later convenience, it is useful to introduce the sets \mathcal{I}_B and \mathcal{I}_P containing, respectively, the bound and the predissociated rovibrational energy levels of N_2 . These satisfy the relations $\mathcal{I}_B \cup \mathcal{I}_P = \mathcal{I}_{BP}$ and $\mathcal{I}_B \cap \mathcal{I}_P = \emptyset$. When the i notation is used, the degeneracy of the rovibrational energy level i is written as $g_i = (2J(i) + 1) g_i^{\text{NS}}$.

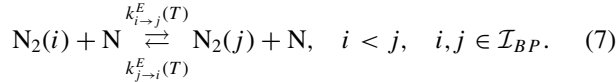
The NASA Ames database for the N_2 -N system comprises more than 20 million reactions in total for three types of processes: (i) collisional dissociation of bound and predissociated states,



(ii) spontaneous predissociation, or tunneling, of predissociated states,



and (iii) collisional excitation between all states,



The collisional excitation processes include the contribution of both inelastic (nonreactive) and exchange processes as follows:

$$k_{i \rightarrow j}^E(T) = k_{i \rightarrow j}^{\text{IE}}(T) + k_{i \rightarrow j}^{\text{EE}}(T), \quad i < j, \quad i, j \in \mathcal{I}_{BP}. \quad (8)$$

The first term $k_{i \rightarrow j}^{\text{IE}}(T)$ accounts for the contribution due to inelastic processes, where kinetic energy is transferred into internal energy during the collision. The second term $k_{i \rightarrow j}^{\text{EE}}(T)$ accounts for exchange processes and the transfer between kinetic and internal energies occurs via substitution of one bounded atom of the molecule with the colliding partner. The importance of this elementary process on the kinetics of dissociation is discussed in detail in Sec. III A 1.

The exothermic rate coefficients for collisional recombination, inverse predissociation, and collisional deexcitation [$k_i^{\text{Db}}(T)$, $k_i^{\text{Pb}}(T)$ and $k_{j \rightarrow i}^E(T)$, with $i < j$, respectively] can be computed based on microreversibility:

$$\frac{k_i^{\text{Df}}(T)}{k_i^{\text{Db}}(T)} = \frac{[g_N Q_N^T(T)]^2}{g_i Q_{N_2}^T(T)} \exp\left[\frac{-(2E_N - E_i)}{k_B T}\right], \quad i \in \mathcal{I}_{BP}, \quad (9)$$

$$\frac{k_i^{\text{Pr}}(T)}{k_i^{\text{Pb}}(T)} = \frac{[g_N Q_N^T(T)]^2}{g_i Q_{N_2}^T(T)} \exp\left[\frac{-(2E_N - E_i)}{k_B T}\right], \quad i \in \mathcal{I}_P, \quad (10)$$

$$\frac{k_{i \rightarrow j}^E(T)}{k_{j \rightarrow i}^E(T)} = \frac{g_j}{g_i} \exp\left(\frac{E_i - E_j}{k_B T}\right), \quad i, j \in \mathcal{I}_{BP}, \quad (11)$$

$$i < j, \quad i, j \in \mathcal{I}_{BP},$$

where the symbol k_B denotes the Boltzmann's constant and quantity E_N is the formation energy of N. The translational

partition functions are defined as

$$Q_N^T(T) = \left(\frac{2\pi k_B m_N T}{h_P^2}\right)^{3/2},$$

$$Q_{N_2}^T(T) = \left(\frac{2\pi k_B m_{N_2} T}{h_P^2}\right)^{3/2}, \quad (12)$$

where symbol h_P denotes Planck's constant and the quantities m_N and m_{N_2} are, respectively, the masses of N and N_2 . The degeneracy of N is $g_N = 12$ and accounts both for the nuclear and electronic spin contributions.

The cross sections for the processes in Eqs. (5) and (7) have been computed using the quasiclassical trajectory (QCT) method with an analytical potential energy surface (PES) that was fit to accurate quantum chemistry calculations for the N_2 -N system [57–60]. Rate coefficients are available at nine values of the gas translational temperature between 7500 K and 50000 K. Numerical values for the former have been obtained by integrating the QCT cross sections over a Maxwellian velocity distribution function. These data have been fitted to a modified Arrhenius form for interpolation. The maximum error resulting from the fit does not exceed 10%, in correspondence of the nodal values.

The total number of possible combinations for collisional excitation exceeds 44 million processes. Among these, some of the transitions are very unlikely (e.g., inelastic excitation for which $j \gg i$) or forbidden by quantum mechanical arguments (ΔJ is odd for inelastic collisions). In this work, the most relevant processes have been included based on the analysis of the results of the QCT calculations. Notice that both endothermic (excitation) and exothermic (deexcitation) processes are found in the database. The number of exothermic processes, about 13.5 million, is larger than the number of endothermic processes (only 7.1 million). A reduced number of transitions (about 1.5 million) include rate coefficients for both types of processes. In this case, the endothermic rate coefficients are preferentially used. In general, we have observed that all the endothermic rate coefficients agree within 70% with the quantities computed by means of the exothermic rate coefficients using micro-reversibility. These discrepancies are due to differences in the statistical sampling errors of the QCT calculations between direct and reverse processes. We have found the results of the master equation calculations to be insensitive to the rate coefficients selected when data from both processes are available.

B. Flow governing equations: Standing shock wave

The nonequilibrium flow behind a normal shock wave is computed under the following assumptions: (i) The flow is steady and one-dimensional, (ii) the flow is inviscid, and (iii) the shock wave moves at a constant speed.

The flow problem is conveniently studied in the shock reference frame. The shock front is treated as a mathematical discontinuity in that the flow quantities experience a discrete jump when crossing the shock. The governing equations for the problem under investigation are the steady, one-dimensional Euler equations.

The global momentum conservation equation is as follows:

$$\frac{d}{dx}(\rho u^2 + p) = 0, \quad (13)$$

where the quantities ρ , u , and p are, respectively, the mixture mass density, velocity, and pressure. The mass density is computed based on the relation $\rho = n_{N_2}m_{N_2} + n_N m_N$, where quantities n_N and n_{N_2} are, respectively, the number densities of N and N_2 . The global energy conservation equation is as follows:

$$\frac{d}{dx}(\rho u H) = 0, \quad (14)$$

where the total enthalpy density is $\rho H = \rho e^T + \rho e^I + \rho e^F + p + \frac{1}{2}\rho u^2$, with the translational, internal, and formation energy densities being equal to $\rho e^T = 3/2(n_{N_2} + n_N)k_B T$,

$\rho e^I = \sum_{i \in \mathcal{I}_{BP}} n_i E_i$ and $\rho e^F = n_N E_N$, respectively. The mixture pressure is computed based on the relation $p = \frac{2}{3}\rho e^T$.

1. Rovibrational collisional model

In the RVC model, each rovibrational level of N_2 is treated as a separate species. Hence, in order to predict the flow field behind the shock, one must couple the global momentum and global energy conservation Eqs. (13) and (14) with the species continuity equations for N and the rovibrational levels of N_2 ,

$$\frac{d}{dx}(n_N u) = \frac{\omega_N}{m_N}, \quad (15)$$

$$\frac{d}{dx}(n_i u) = \frac{\omega_i}{m_{N_2}}, \quad i \in \mathcal{I}_{BP}. \quad (16)$$

The production rates for N and for the rovibrational energy levels of N_2 due to collisional dissociation and excitation, and predissociation (and the related reverse exothermic processes) can be computed based on the zeroth-order reaction rate theory [6,66]:

$$\omega_N = 2m_N n_N \sum_{i \in \mathcal{I}_{BP}} [n_i k_i^{\text{Df}}(T) - n_N^2 k_i^{\text{Db}}(T)] + 2m_N \sum_{i \in \mathcal{I}_P} [n_i k_i^{\text{Pf}}(T) - n_N^2 k_i^{\text{Pb}}(T)], \quad (17)$$

$$\begin{aligned} \omega_i = m_{N_2} n_N \sum_{\substack{j \in \mathcal{I}_{BP} \\ j > i}} [n_j k_{j \rightarrow i}^E(T) - n_i k_{i \rightarrow j}^E(T)] - m_{N_2} n_N \sum_{\substack{j \in \mathcal{I}_{BP} \\ j < i}} [n_j k_{i \rightarrow j}^E(T) - n_i k_{j \rightarrow i}^E(T)] \\ - \begin{cases} m_{N_2} n_N [n_i k_i^{\text{Df}}(T) - n_N^2 k_i^{\text{Db}}(T)] + m_{N_2} [n_i k_i^{\text{Pf}}(T) - n_N^2 k_i^{\text{Pb}}(T)], & i \in \mathcal{I}_{BP}, \\ m_{N_2} n_N [n_i k_i^{\text{Df}}(T) - n_N^2 k_i^{\text{Db}}(T)], & i \in \mathcal{I}_B. \end{cases} \end{aligned} \quad (18)$$

In order to characterize macroscopically thermal nonequilibrium effects when using the RVC model, internal, rotational, and vibrational temperatures are extracted from the rovibrational populations based on the following implicit relations:

$$\sum_{i \in \mathcal{I}_{BP}} n_i E_i - n_{N_2} E_{N_2}^I(T^I) = 0, \quad (19)$$

$$\sum_{\substack{v \in \mathcal{V} \\ J \in \mathcal{J}_v}} n_{vJ} \Delta \tilde{E}_v(J) - n_{N_2} E_{N_2}^R(T^R, T^V) = 0, \quad (20)$$

$$\sum_{v \in \mathcal{V}} \tilde{n}_v \tilde{E}_v - n_{N_2} E_{N_2}^V(T^R, T^V) = 0. \quad (21)$$

The number density of the vibrational level v is computed by summing the individual contributions of all of its rotational levels, $\tilde{n}_v = \sum_{J \in \mathcal{J}_v} n_{vJ}$. The (partial) equilibrium internal, rotational, and vibrational energies (per molecule) are defined as follows:

$$E_{N_2}^I(T^I) = k_B T^{I2} \frac{\partial \ln Q_{N_2}^I(T^I)}{\partial T^I}, \quad (22)$$

$$E_{N_2}^R(T^R, T^V) = k_B T^{R2} \frac{\partial \ln Q_{N_2}^I(T^R, T^V)}{\partial T^R}, \quad (23)$$

$$E_{N_2}^V(T^R, T^V) = k_B T^{V2} \frac{\partial \ln Q_{N_2}^I(T^R, T^V)}{\partial T^V}, \quad (24)$$

where the one- and two-temperature internal partition functions are

$$Q_{N_2}^I(T^I) = \sum_{i \in \mathcal{I}_{BP}} g_i \exp\left(-\frac{E_i}{k_B T^I}\right), \quad (25)$$

$$Q_{N_2}^I(T^R, T^V) = \sum_{\substack{v \in \mathcal{V} \\ J \in \mathcal{J}_v}} g_{vJ} \exp\left[-\frac{\tilde{E}_v}{k_B T^V} - \frac{\Delta \tilde{E}_v(J)}{k_B T^R}\right]. \quad (26)$$

The flow field behind the shock is obtained by solving numerically Eqs. (13), (14), (15), and (16). The solution initial value is obtained by means of the Rankine-Hugoniot jump relations (with the assumption of frozen dissociation and excitation within the shock). The population of the rovibrational levels immediately behind the shock is assumed to follow a Maxwell-Boltzmann distribution as follows:

$$\frac{n_i}{n_{N_2}} = \frac{g_i}{Q_{N_2}^I(T^I)} \exp\left(\frac{-E_i}{k_B T^I}\right), \quad i \in \mathcal{I}_{BP}, \quad (27)$$

where the internal temperature is set equal to the adopted free-stream temperature value. Due to the typical stiffness of chemical kinetics problems, the numerical integration of Eqs. (13), (14), (15), and (16) is performed by means of the

backward-differentiation-formula (BDF) implicit methods as implemented in the LSODE library [67].

2. Vibrational collisional model

The vibrational collisional (VC) model has been developed based on the RVC model described in Sec. II B 1 and relies on the simplifying assumption of equilibrium (Maxwell-Boltzmann) distribution of the rotational levels [16,18],

$$\frac{n_{vJ}}{\tilde{n}_v} = \frac{g_{vJ}}{\tilde{Q}_v(T_v^R)} \exp\left[-\frac{\Delta\tilde{E}_v(J)}{k_B T_v^R}\right], \quad v \in \mathcal{V}, \quad J \in \mathcal{J}_v, \quad (28)$$

where the rotational partition function of the vibrational level v is defined as $\tilde{Q}_v(T_v^R) = \sum_{J \in \mathcal{J}_v} g_{vJ} \exp[-\Delta\tilde{E}_v(J)/(k_B T_v^R)]$. In the VC model predissociation is not taken into account and it is further assumed (as often done in the literature [21,68]) that *rotation and translation are in equilibrium* (i.e., $T_v^R = T$, $v \in \mathcal{V}$).

The set of master equation for the VC model can be obtained by substituting Eq. (28) (with $T_v^R = T$) in Eqs. (17) and (18) and summing over the rotational levels of each vibrational state as follows:

$$\frac{d}{dx}(n_N u) = \frac{\omega_N}{m_N}, \quad (29)$$

$$\frac{d}{dx}(\tilde{n}_v u) = \frac{\tilde{\omega}_v}{m_{N_2}}, \quad v \in \mathcal{V}. \quad (30)$$

The production rates of N and the vibrational levels of N_2 are

$$\omega_N = 2m_N n_N \sum_{v \in \mathcal{V}} [\tilde{n}_v \tilde{k}_v^{\text{Df}}(T) - \tilde{k}_v^{\text{Db}} n_N^2(T)], \quad (31)$$

$$\begin{aligned} \tilde{\omega}_v &= m_{N_2} n_N \sum_{\substack{w > v \\ w \in \mathcal{V}}} [\tilde{n}_w \tilde{k}_{vw}^E(T) - \tilde{n}_v \tilde{k}_{vw}^E(T)] \\ &\quad - m_{N_2} n_N \sum_{\substack{w < v \\ w \in \mathcal{V}}} [\tilde{n}_w \tilde{k}_{vw}^E(T) - \tilde{n}_v \tilde{k}_{vw}^E(T)] \\ &\quad - m_{N_2} n_N [\tilde{n}_v \tilde{k}_v^{\text{Df}}(T) - n_N^2 \tilde{k}_b^{\text{Db}}(T)], \quad v \in \mathcal{V}. \end{aligned} \quad (32)$$

The vibrational dissociation and excitation rate coefficients [$\tilde{k}_v^{\text{Df}}(T)$ and $\tilde{k}_{vw}^E(T)$, with $v < w$, respectively], and those of the related exothermic processes, can be obtained by averaging over the rotational levels the elementary rovibrational rate coefficients. Their mathematical expressions [obtained from the algebraic manipulation leading to Eqs. (29) and (30) are provided in Appendix A].

For the VC model, due to the assumption of thermal equilibrium between rotation and translation, the internal energy density of N_2 [to be used in Eq. (14)] becomes

$$\rho e^I = \sum_{v \in \mathcal{V}} \tilde{n}_v \left[\tilde{E}_v + k_B T^2 \frac{\partial \ln \tilde{Q}_v(T)}{\partial T} \right]. \quad (33)$$

The flow field behind the shock wave is computed by applying the same procedure as for the RVC model (Sec. II B 1), with the difference that the postshock conditions are obtained by imposing rotational equilibrium within the shock. The population of the vibrational levels immediately behind the

shock is assumed to follow a Maxwell-Boltzmann distribution,

$$\frac{\tilde{n}_v}{n_{N_2}} = \frac{\tilde{Q}_v(T)}{Q_{N_2}^I(T, T^V)} \exp\left(\frac{-\tilde{E}_v}{k_B T^V}\right), \quad v \in \mathcal{V}, \quad (34)$$

where the vibrational temperature is set equal to the adopted free-stream temperature value.

3. Multitemperature model

The multitemperature (MT) model used in the present work is based on the thermodynamic and kinetic data of the NASA Ames database and has been developed by Panesi *et al.* [33] by means of isothermal heat bath calculations. The MT model allows for the existence of rotational and vibrational temperatures. The study of the flow behind the shock wave is performed by coupling the global momentum and global energy conservation Eqs. (13) and (14) with the species continuity equation for N and N_2 , and the rotation and vibrational energy conservation equations,

$$\frac{d}{dx}(n_N u) = \frac{\omega_N}{m_N}, \quad (35)$$

$$\frac{d}{dx}(n_{N_2} u) = \frac{\omega_{N_2}}{m_{N_2}}, \quad (36)$$

$$\frac{d}{dx}(n_{N_2} m_{N_2} E_{N_2}^R u) = \frac{1}{m_{N_2}} (\Omega_{N_2}^{T-R} + \Omega_{N_2}^{D-R}), \quad (37)$$

$$\frac{d}{dx}(n_{N_2} m_{N_2} E_{N_2}^V u) = \frac{1}{m_{N_2}} (\Omega_{N_2}^{T-V} + \Omega_{N_2}^{D-V}). \quad (38)$$

The production rates of N and N_2 are as follows:

$$\omega_N = 2m_N n_N [n_{N_2} k_{\text{QSS}}^{\text{Df}}(T) - n_N^2 k^{\text{Db}}(T)], \quad (39)$$

$$\omega_{N_2} = -m_{N_2} n_N [n_{N_2} k_{\text{QSS}}^{\text{Df}}(T) - n_N^2 k^{\text{Db}}(T)], \quad (40)$$

where QSS indicates that the macroscopic dissociation rate coefficient has been extracted at quasi-steady-state conditions [33]. The macroscopic recombination rate coefficients is obtained via microreversibility,

$$\frac{k_{\text{QSS}}^{\text{Df}}(T)}{k^{\text{Db}}(T)} = \frac{[g_N Q_N^T(T)]^2}{Q_{N_2}^T(T) Q_{N_2}^I(T)} \exp\left(\frac{-2E_N}{k_B T}\right). \quad (41)$$

The energy source terms on the right-hand-side of Eqs. (37) and (38) account for the creation or destruction of rotational and vibrational energy due to collisional excitation ($\Omega_{N_2}^{T-R}$ and $\Omega_{N_2}^{T-V}$) and dissociation ($\Omega_{N_2}^{D-R}$ and $\Omega_{N_2}^{D-V}$). The dependence of the aforementioned quantities on the gas macroscopic properties (such as temperature and chemical composition) have been obtained based on isothermal heath bath calculations [33] (the detailed expressions are provided in Appendix B).

For the MT model, due to the assumption of (partial) equilibrium of rotational and vibrational energy models, the internal energy density of N_2 [to be used in Eq. (14)] becomes

$$\rho e^I = n_{N_2} E_{N_2}^R(T^R, T^V) + n_{N_2} E_{N_2}^V(T^R, T^V). \quad (42)$$

The flow field immediately behind the shock wave is initialized by applying the Rankine-Hugoniot jump relations (where the rotational and vibrational temperature are both frozen within the shock).

TABLE I. Translational temperature, pressure, velocity, and nitrogen atom mole fraction for a N_2 -N mixture in the ground electronic state [the first column indicates the chemical nonequilibrium thermal equilibrium conditions in the free-stream (∞)]; “RVC and MT” indicates the postshock nonequilibrium conditions at the shock location for the RVC and MT models; “VC” indicates the postshock nonequilibrium conditions at the shock location for the VC model; “LTE” indicates the local thermodynamic equilibrium postshock conditions).

	∞	RVC and MT	VC	LTE
T (K)	300	62 546	46 759	11 351
p (Pa)	13.33	10 792	12 275	13 363
u (km/s)	10	2.51	1.69	0.72
X_N	0.028	0.028	0.028	1

III. RESULTS AND DISCUSSION

The nonequilibrium thermodynamic state of the shock heated nitrogen gas is analyzed in detail over the next sections. The N_2 -N gas mixture is assumed to be in chemical nonequilibrium and thermal equilibrium in the free-stream (∞) at $p_\infty = 0.1$ torr (13.33 Pa) and $T_\infty = 300$ K. A chemical nonequilibrium value of 2.8% mole fraction of N was chosen to have enough nitrogen atoms in the flow, since only N_2 -N collisions are considered in this work. The postshock conditions for the three nonequilibrium models (RVC, VC, and MT) are computed as explained in Sec. (II B). The related numerical values for pressure, temperature, and velocity are provided in Table I, together with the postshock local thermodynamic equilibrium (LTE) conditions. In the present analysis, the shock location is always fixed at the origin of the reference frame ($x = 0$ m).

A. Postshock relaxation: Rovibrational collisional model

1. Nonequilibrium thermodynamic properties

This section characterizes the nonequilibrium state of the gas behind a strong shock wave in terms of macroscopic thermodynamic quantities. For this purpose, we use the RVC model to analyze the evolution of the temperature and composition in the postshock nonequilibrium relaxation for a

wide range of flow conditions. The influence of exchange and dissociation processes on the macroscopic flow quantities in the postshock relaxation region is also discussed.

Figure 1(a) shows the translational and the internal temperatures as a function of the distance from the shock for the RVC model. It is important to note that the internal temperature has been computed in the postprocessing phase [through Eq. (19)], as discussed by Panesi *et al.* [33]. The cooling of the translational temperature is caused by the excitation of the internal energy modes and by the onset of the chemical reactions. This can be easily confirmed by inspection of the dynamics of the internal temperature in Fig. 1(a) and by the evolution of the mole fraction of atomic nitrogen shown (with solid line) in Fig. 1(b). The distance required to achieve complete equilibration slightly exceeds 0.02 m. However, the thermal equilibrium is already achieved in the near-shock region (after only 0.005 m).

Exchange processes play a fundamental role in the energy transfer and dissociation processes as already discussed by Panesi *et al.* [33]. In an exchange process, one of the atoms of the N_2 molecule is replaced by the free atom participating to the collision. As a consequence, the product molecule has no memory of the initial state of excitation and can assume a broad distribution of energy levels, compatible with the total energy of the collision. This is not the case for inelastic transitions, which are also subject to the selection rule that constrains ΔJ to be even. In order to assess the relative importance of the two channels, we analyze the results of relaxation with and without exchange reactions. Figure 1 shows the influence that these processes have on temperatures and the N mole fraction. When exchange processes are not taken into account, the relaxation distance is roughly doubled, as shown in Fig. 1(a). Thus, neglecting the exchange processes lowers the excitation rate of nitrogen molecules which, in turn, slows down the dissociation.

Figure 2 shows the influence of predissociation on the temperatures and the N mole fraction. Predissociation has the effect of decreasing the dissociation rate of N_2 . However, its influence on the relaxation dynamics appears negligible, especially when compared with the effects of the exchange processes. The same conclusion holds also for other flow quantities, such as velocity, pressure, etc., not shown in Fig. 2.

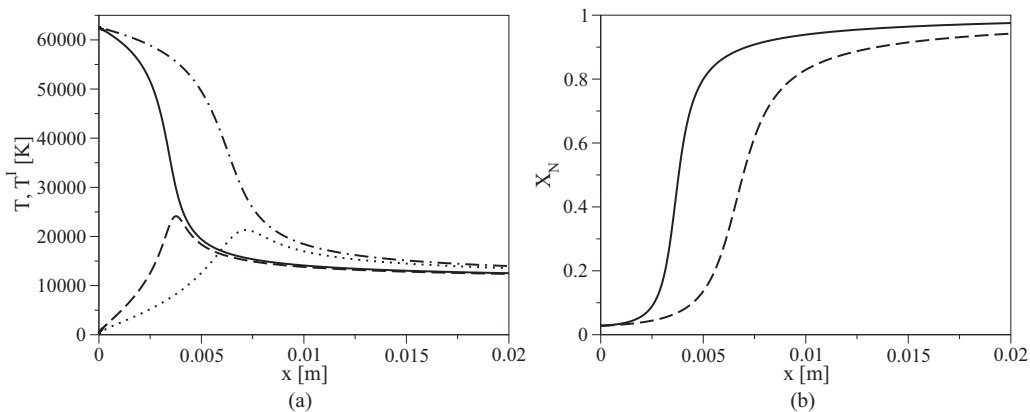


FIG. 1. RVC model. Temperature (a) and N mole fraction (b) evolution behind the shock wave with or without exchange processes [$p_\infty = 0.1$ torr and $u_\infty = 10$ km/s; in (a) unbroken line, T with exchange; dashed line, T' with exchange; dotted-dashed line, T without exchange; dotted line, T' without exchange; in (b) unbroken line, with exchange; dashed line, without exchange].

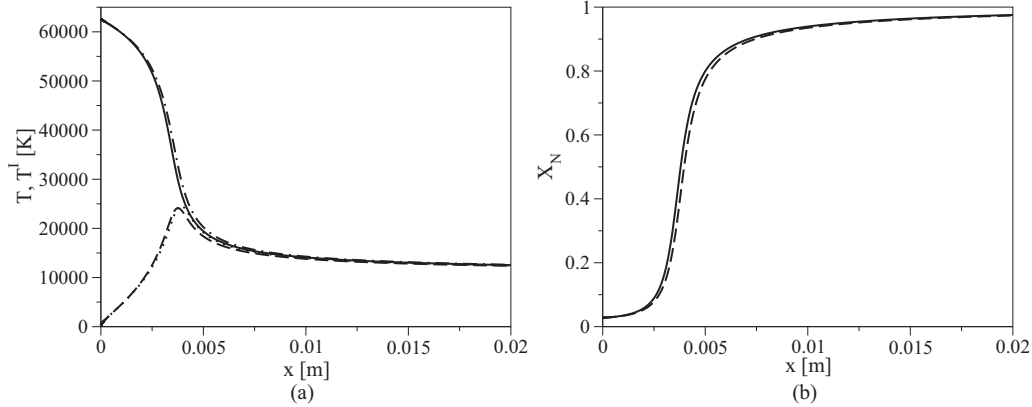


FIG. 2. RVC model. Temperature (a) and N mole fraction (b) evolution behind the shock wave with or without predissociation [$p_\infty = 0.1$ torr and $u_\infty = 10$ km/s; in (a) unbroken line, T with predissociation; dashed line, T^I with predissociation; dotted-dashed line, T without predissociation; dotted line, T^I without predissociation; in (b) unbroken line, with predissociation; dashed line, without predissociation].

We conclude this section with the analysis of the behavior of the rotational and vibrational excitation of the $N_2(^1\Sigma_g^+)$ molecules in the postshock region. In order to characterize the influence of shock velocity on the extent of nonequilibrium in the gas, we have investigated the postshock relaxation for shock speeds ranging from 4 to 10 km/s. The results of the analysis are shown in Fig. 3.

The characterization of excitation of the molecules is obtained by plotting the rotational and vibrational temperatures extracted by the population distributions obtained from the RVC model. These temperatures are roughly proportional to the instantaneous average rotational and vibrational energies at each position after the shock and can be used to characterize the average state of excitation of the $N_2(^1\Sigma_g^+)$ molecules.

The analysis of the temperature evolution demonstrates how both rotation and vibration are found in strong nonequilibrium conditions for large portion of the thermochemical relaxation. Furthermore, their rates of relaxation are comparable for the 6- and 10-km/s conditions. The only condition for which rotation is significantly faster than vibration is 4 km/s. It is important to mention that these conditions are of limited interest to the scientific community since the nonequilibrium effects (or high-

temperature effects, in general) have been proven to have a limited influence on the flow quantities.

In the literature, several studies have addressed the modeling of rotational nonequilibrium: For example, Olynyk and Hassan [69], Holman and Boyd [70], and Deschenes *et al.* [71] have used Parker's model [72] and the Landau-Teller relaxation form to describe rotational nonequilibrium effects. More recently, Kim and Boyd [20] have used a three-temperature model (partially derived using *ab initio* data) to study the nonequilibrium relaxation behind a standing shock wave. All these analyses rely on the assumption of the Maxwell-Boltzmann population distribution of the internal energy levels. In the next sections we will show that this assumption does not hold in nonequilibrium conditions of interest. Furthermore, Parker's model was derived by using a overly simplified description of the molecular collisions and the result obtained with this model cannot be conclusive.

2. Rovibrational energy level dynamics

The analysis proceeds with the investigation of the behavior of the internal rovibrational levels in the post shock relaxation

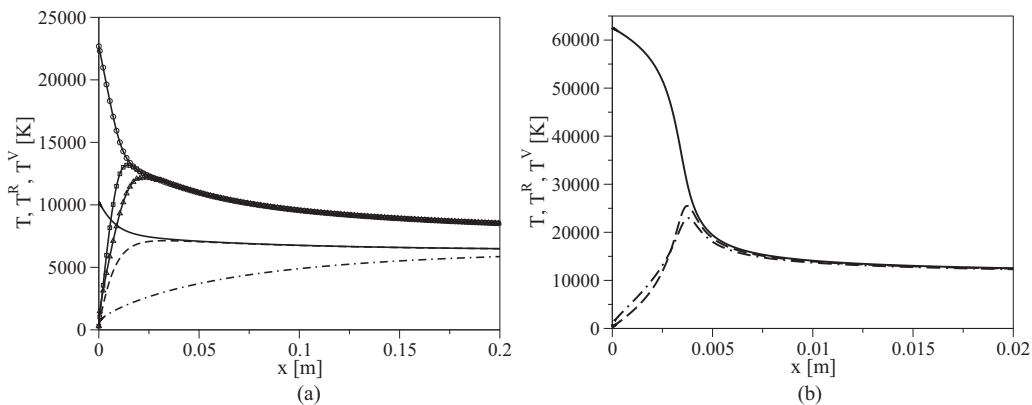


FIG. 3. RVC model. Comparative evolution of the translational, rotational, and vibrational temperatures behind the shock wave ($p_\infty = 0.1$ torr). (a) Lines with symbols refer to the $u_\infty = 6$ (km/s) case. In this case, the circles indicate T , squares T^R , and triangles T^V . The simple lines refers to the $u_\infty = 4$ (km/s) case. In this case, the solid line indicates T , dashed-line T^R , and dot-dashed line T^V . (b) The $u_\infty = 10$ (km/s) case. The solid line indicates T , dashed-line T^R , and dot-dashed line T^V .

TABLE II. RVC model. Position, N mole fraction, and temperatures for the locations where the population distributions are extracted.

No.	x (m)	t (s)	N	T (K)	T^I (K)	T^R (K)	T^V (K)
1	2.5×10^{-5}	1.0×10^{-9}	2.8×10^{-2}	62 486	473	375	947
2	2.5×10^{-4}	1.0×10^{-7}	2.9×10^{-2}	61 926	1595	1059	2269
3	2.3×10^{-3}	1.0×10^{-6}	7.5×10^{-2}	53 205	11 232	10 367	11 964
4	3.2×10^{-3}	1.5×10^{-6}	2.3×10^{-1}	40 637	19 953	20 771	19 275
5	3.4×10^{-3}	1.6×10^{-6}	3.2×10^{-1}	36 297	22 291	23 565	21 210
6	3.6×10^{-3}	1.7×10^{-6}	4.1×10^{-1}	32 481	23 748	25 185	22 506
7	3.9×10^{-3}	1.9×10^{-6}	5.4×10^{-1}	27 794	23 891	25 092	22 850
8	5.1×10^{-3}	3.0×10^{-6}	8.1×10^{-1}	18 987	18 016	18 408	17 696

zone. To this aim, we have extracted the level populations for eight locations in the postshock region. The corresponding distances from the shock, Lagrangian times, temperatures and compositions are indicated in Table II.

Immediately behind the shock, most of the nitrogen molecules in the flow occupy the lower rovibrational energy levels. Over 99% of the molecules are found in the ground vibrational state and only the low-lying rotational levels are significantly populated. With time, the thermal motion of molecules brings about collisions, thus enabling the transfer of kinetic energy into rotational and vibrational energy. As a result, in the early stages of the relaxation, the population of the internal levels strongly departs from equilibrium distribution and the dynamics of each level is governed by its own kinetics, as shown by Fig. 4(b).

The behavior of the rovibrational level population depends upon their energy and their quantum state, uniquely characterized by the vibrational and rotational quantum numbers. Thus, three different groups of levels can be identified in Fig. 4(a): the *low-lying*, *intermediate*, and *high-lying* rovibrational levels.

At the beginning of the relaxation, the molecules in the lower vibrational and rotational levels (0 to 2.5 eV) still follow a Maxwell-Boltzmann distribution at the free-stream temperature. As the relaxation evolves, they slowly thermalize to the instantaneous translational temperature. The analysis of the evolution of N concentration [in Fig. 4(a)] shows that the relaxation process for the low-lying levels has not completed when the molecules start to undergo dissociation.

The intermediate levels (2.5 to 9 eV) appear to be thermalized at a common temperature, which is closer to the instantaneous translational temperature. Their relaxation rate appears significantly faster with respect to the low-lying levels. In the early stages of the relaxation (2.5×10^{-5} – 2.5×10^{-4} s) the population of the intermediate levels, characterized by similar internal energy, spans several orders of magnitude, while, as the relaxation proceeds further, they quickly thermalize at a Maxwell-Boltzmann distribution, identified by a straight line in the Boltzmann plot.

The quasibound levels (>9 eV) behave differently from the intermediate ones. The reason for this behavior is twofold: they exhibit different excitation dynamics and, due to their finite lifetime, they have the additional spontaneous dissociation channel. Their excitation kinetics proceeds from the low-lying vibrational levels by following a ladder-climbing process within their rotational structure. This is because the quasibound levels are characterized by high rotational and low vibrational energy, as opposed to the high-lying bound levels (with $v \gg 1$), which tend to store energy in the vibrational energy mode. Thus, the probability of energy transfer between quasibound and high-lying vibrational states is low, and hinders the thermalization process. Because of their different dynamics, the quasibound levels strongly depart from the equilibrium distribution. Furthermore, the majority of them dissociate by quantum tunneling. The short-lived ones are strongly depleted and can be safely neglected, since they play a very small role in the relaxation. In general, due to their large

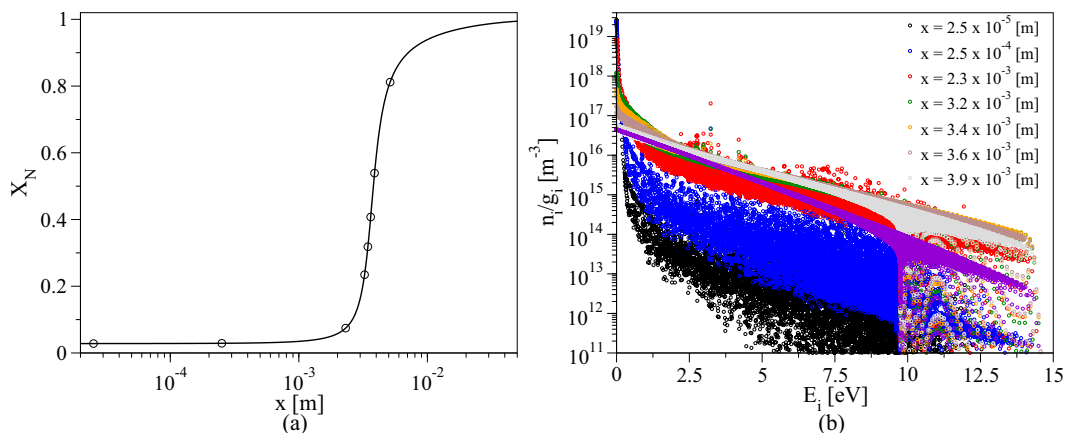


FIG. 4. (Color online) RVC model. Comparative evolution of the N mole fraction (a) and rovibrational energy level distribution (b) behind the shock wave [$p_\infty = 0.1$ torr and $u_\infty = 10$ km/s; the symbols in (a) highlight the locations at which the population distributions, plotted in (b), are extracted].

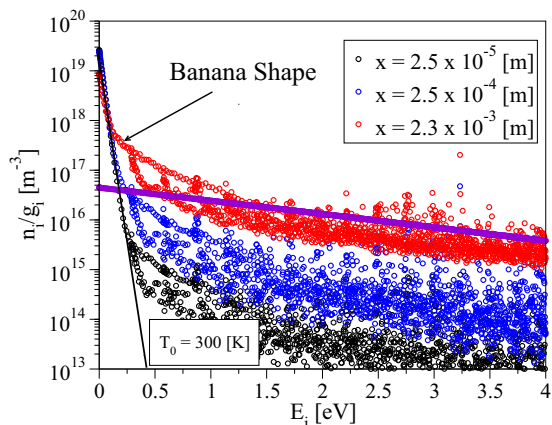


FIG. 5. (Color online) RVC model. Evolution behind the shock wave of the population of the rovibrational energy levels lying close to the ground state ($p_\infty = 0.1$ torr and $u_\infty = 10$ km/s; the locations at which the distributions are plotted are the same as those of Fig. 4).

cross sections for dissociation, the quasibound level population can be obtained assuming chemical equilibrium with the free state (Guldberg and Waage equations [73,74]).

Figure 5 shows the populations of the low-lying states in the early stages of the relaxation. The low-lying levels are frozen at T_0^I and the populations of higher levels (intermediate and high-lying levels) steadily increase, displaying a characteristic “banana shape.” As the relaxation proceeds further, part of the gas reaches a state of partial equilibrium, during which the population is dissected into separate strands for each low-lying v , while the intermediate levels have already thermalized at the translational temperature, T . This is a manifestation of the faster equilibration of rotation at lower temperatures.

To better clarify this idea, the rovibrational population of the first four vibrational levels is shown in Fig. 6. The bound levels relax toward equilibrium through series of partial equilibrium rotational distributions, so the molecules in the same vibrational quantum state v are populated according to a Maxwell-Boltzmann distribution at a common rotational temperature. The rotational temperature of the low-lying vibrational states ($0 < v < 5$) is lower than T and steadily

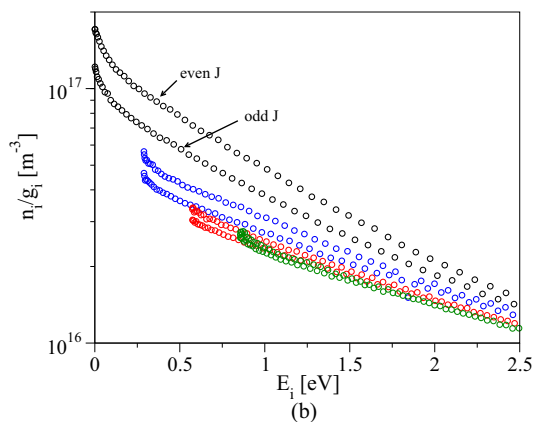
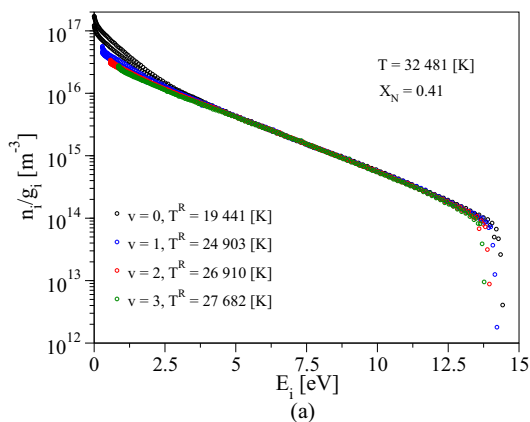


FIG. 6. (Color online) RVC model. Rotational energy level distribution for the ground and the first three excited vibrational states at $x = 3.6 \times 10^{-3}$ m behind the shock wave [$p_\infty = 0.1$ torr and $u_\infty = 10$ km/s; global view (a) and zoom around the ground state (b)].

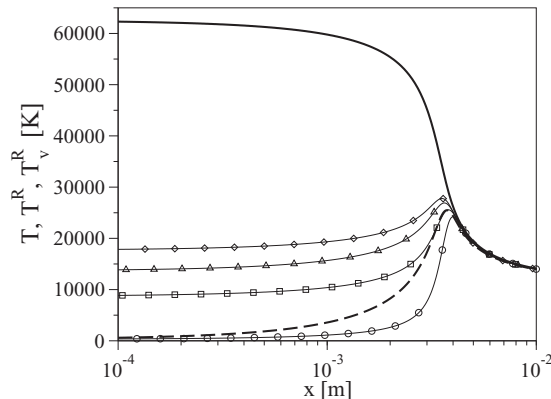


FIG. 7. RVC model. Translational and rotational temperature evolution behind the shock wave ($p_\infty = 0.1$ torr and $u_\infty = 10$ km/s; unbroken line, T ; dashed line, T^R ; line with circles, T_0^R ; line with squares, T_1^R ; line with triangles, T_2^R ; line with diamonds T_3^R).

increases with the vibrational quantum number, until $T_v^R = T$ for the higher vibrational levels.

A careful inspection of Fig. 6 demonstrates how the dynamics of the low-lying states strongly depends on whether the rotational quantum number is even or odd. The rotational levels characterized by even quantum number have twice the nuclear spin degeneracy compared to the odd levels [Eq. (2)]. Thus, the total preshock population of $N_2(^1\Sigma_g^+)$ molecules, characterized by even J quantum number, is twice the odd J population. This justifies the splitting of the low-lying energy levels into two strands in the early part of the relaxation. It is important to mention that the population exchange among levels with even and odd rotational quantum number is forbidden by the quantum mechanical selection rules for the energy transfer processes. As a result, the only way to exchange population is via exchange reactions, which, however, are rather inefficient for the low-lying energy levels, due to the higher height of the exchange barrier. Thus, the nonequilibrium population maintains this difference, until the exchange reactions become significant.

The spatial evolution of the rotational temperatures for the first four rotational levels is shown in Fig. 7. In the same figure an averaged rotational temperature is also included.

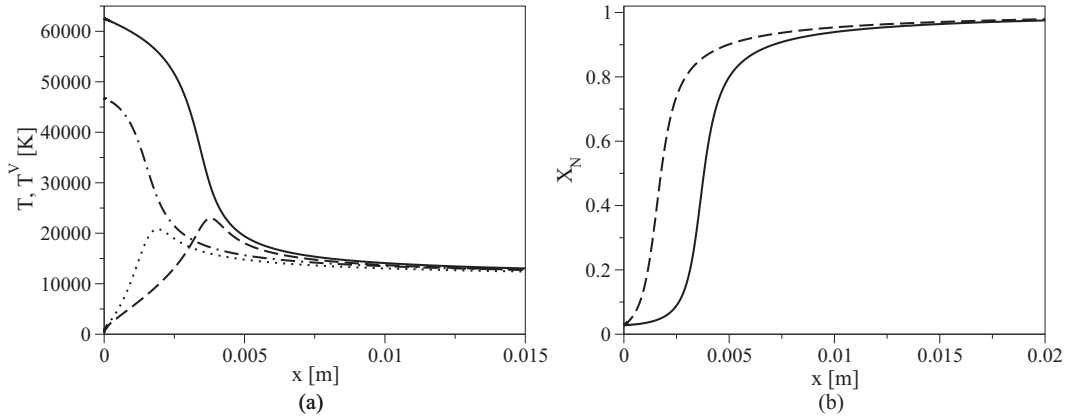


FIG. 8. Comparison of the VC and RVC models. Translational and vibrational temperature (a) and N mole fraction (b) evolution behind the shock wave [$p_\infty = 0.1$ torr and $u_\infty = 10$ km/s; in (a) unbroken line, T RVC; dashed line, T^V RVC; dotted-dashed line, T VC; dotted line, T^V VC; in (b) unbroken line, RVC; dashed line, VC].

After a sharp rise in the rotational temperatures T_v^R , not shown in the figure, the temperatures appear frozen throughout the incubation period, which precedes the onset of dissociation. The dynamics of the averaged rotational temperature is similar to the dynamics of the temperature of the low-lying vibrational levels (e.g., $v = 0, 1$). This is the result of the averaging procedure, which tends to favor the levels characterized by higher population density. All the rotational temperatures significantly depart from the translational temperature until large part of the dissociation has occurred and a state of thermal equilibrium has been achieved. This is an important finding since the equilibration between rotation and translation is often assumed in the multitemperature as well as in the more advanced vibrational collisional models.

B. Comparison of the nonequilibrium models

The nonequilibrium flow behind a strong shock wave is solved using a hierarchy of nonequilibrium models: (1) the MT model, based on the assumption of Maxwell-Boltzmann distribution for the rovibrational levels of N_2 [33]; (2) the VC model, which allows for the nonequilibrium population of the vibrational levels retains the assumption of equilibrium population for the rotational levels with $T^R = T$; and (3) the RVC model, which is free of simplifying assumptions concerning the internal level populations. Both the VC and the MT models can be obtained directly from the RVC models by taking moments of the master equations [18,33]. All the models rely on the same *ab initio* kinetic database discussed in Sec. II A. Thus, the differences in the calculations observed in the results presented can be attributed to the differences in the fundamental assumptions adopted by the nonequilibrium models. Furthermore, the use of a unique database across the different models implies that the results obtained with the RVC model can be taken as a reference and considered more accurate, since it is based on a reduced number of simplifying assumptions.

Figure 8 shows a comparison of the temperature and N mole fraction profiles in the postshock region obtained by using the VC and the RVC models. The main difference between the VC and the RVC model is the assumption that each rotational level is populated according to a Maxwell-Boltzmann distribution

at $T = T_v^R$. This assumption is responsible for the differences observed in Fig. 8. When crossing the shock, the equilibration of translational and rotational energy modes causes a significant lowering of the postshock translational temperature due to the higher heat capacity of the gas. This explains the difference between the initial translational temperatures of the RVC and the VC models, shown in Fig. 8(a). Furthermore, in the VC model, the elevated rotational temperature, encountered in the postshock region, significantly enhances the dissociation rate and promote a faster thermal and chemical relaxation of the gas to the final equilibrium condition.

Figure 9 compares the temperatures and mole fractions predicted by the RVC and MT models. In the case of the RVC model, the rotational and vibrational temperatures shown in Fig. 9(a) have been computed in the postprocessing phase [through Eqs. (20) and (21)], as discussed by Panesi *et al.* [33]. These temperatures give an idea of the average energy content of the gas in the rotational and vibrational energy modes, respectively. However, their physical significance is limited, since for the RVC model, the rotational and vibrational distributions strongly depart a Maxwell-Boltzmann distribution.

The thermal relaxation obtained with MT model appears significantly faster than the RVC result as will be discussed in the next sections. The spatial evolution of the atomic concentration is shown in Fig. 9. The time required for the atomic concentration to reach 80% of its final value, for the MT model, is about half the time needed by the RVC model. This result has been observed shock speeds ranging from 6 to 11 km/s.

Thus, the MT model predictions are in close agreement with the VC results in terms of temperature evolution and composition profiles. Both models tend to overestimate the dissociation rate, thus leading to faster production of atomic nitrogen and to a faster cooling of the translational temperature. The reason for this finding is discussed in the next section.

C. Dissociation rates and dynamics of dissociation

The previous sections have shown a comparison of the MT and VC predictions with ones obtained by using the RVC model. The disagreement between the simplified MT and VC models and the RVC model is further investigated in

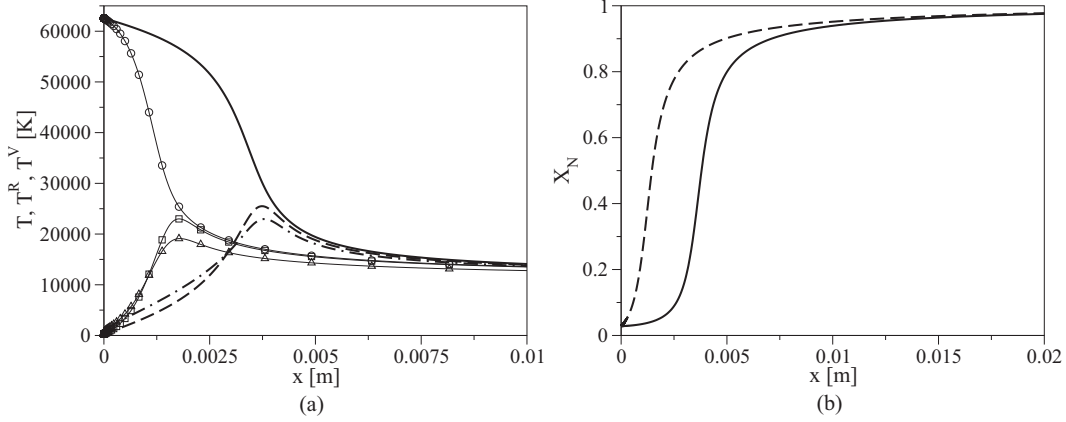


FIG. 9. RVC and MT model comparison. Temperature and N mole fraction evolution behind the shock wave [$p_\infty = 0.1$ torr and $u_\infty = 10$ km/s; in (a) unbroken line, T RVC; dashed line, T^R RVC; dotted-dashed line, T^V RVC; line with circles, T MT; line with squares, T^R MT; line with triangles, T^V MT; in (b) unbroken line, RVC; dashed lines, MT].

this section through the analysis of the dissociation kinetics. The reasons behind the inabilities of the reduced models to capture the dynamics of N_2 dissociation differ in the two cases. The in-depth analysis of the dissociation kinetics for the MT models is discussed in Sec. III C 1, while the one for the VC models is discussed in Sec. III C 2.

1. Dissociation dynamics predicted by the MT model

In order to understand the possible sources for this systematic discrepancy between the RVC and MT models, the mass production and energy transfer terms have been extracted from the RVC and MT solutions and are shown in Fig. 10. The results suggest that the MT model fails to predict the correct thermochemical relaxation, due an overestimation of the macroscopic dissociation rate. The interpretation of the energy relaxation source terms is more difficult due to the influence of the chemistry on the energy transfer processes.

In order to isolate the major contribution to the relaxation of energy transfer ($\Omega_{N_2}^{T-R}$ and $\Omega_{N_2}^{T-V}$) and chemistry energy coupling ($\Omega_{N_2}^{D-R}$ and $\Omega_{N_2}^{D-V}$), we have repeated the simulation ex-

cluding the dissociation processes from the models. Figure 11 shows a comparison between the temperature fields obtained with the MT and RVC models. In this case, the agreement between the two predictions is excellent. Thus, the nonreactive energy transfer source terms in the MT energy equations seem to correctly capture the dynamics of the energy transfer.

The shortcoming of the MT model is due to its inability to correctly model the N_2 dissociation rate using a phenomenological (or macroscopic) dissociation rate coefficient. Only in the presence of a quasi-steady-state (QSS) distribution, among the internal energy levels, is it possible to define a macroscopic reaction rate coefficient, as discussed by Park [75]. In the present work, the derivation of the rate coefficient for dissociation is obtained from the study of the relaxation of nitrogen molecules in a 0D isothermal chemical reactor, as discussed by Panesi *et al.* [33].

The macroscopic rate coefficient k^{Df} is defined as follows:

$$k^{Df}(T) = \sum_{i \in \mathcal{L}_{BP}} \frac{n_i k_i^{Df}(T)}{n_{N_2}}. \quad (43)$$

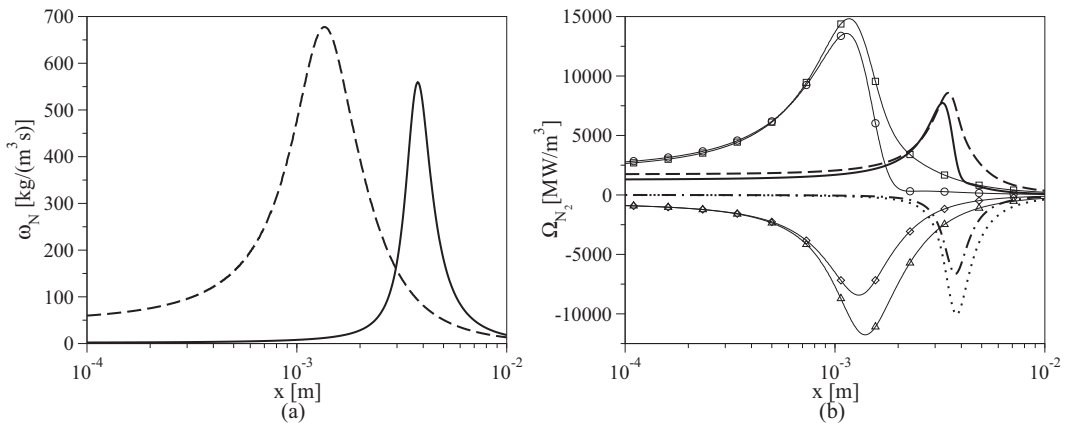


FIG. 10. RVC and MT model comparison. Mass production (a) and energy transfer (b) term evolution behind the shock wave [$p_\infty = 0.1$ torr and $u_\infty = 10$ km/s; in (a) unbroken line, RVC; dashed line, MT; in (b) unbroken line, $\Omega_{N_2}^{T-R}$ RVC; dashed line, $\Omega_{N_2}^{T-V}$ RVC; dotted-dashed line, $\Omega_{N_2}^{D-R}$ RVC; dotted line, $\Omega_{N_2}^{D-V}$ RVC; line with circles, $\Omega_{N_2}^{T-R}$ MT; line with squares, $\Omega_{N_2}^{T-V}$ MT; line with triangles, $\Omega_{N_2}^{D-R}$ MT; line with diamonds, $\Omega_{N_2}^{D-V}$ MT].

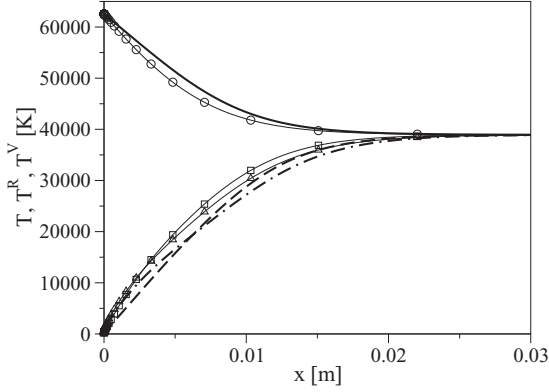


FIG. 11. RVC and MT model comparison. Temperature evolution behind the shock wave switching off dissociation [$p_\infty = 0.1$ torr and $u_\infty = 10$ km/s; unbroken line, T RVC; dashed line, T^R RVC; dotted-dashed line, T^V RVC; line with circles, T MT; line with squares, T^R MT; line with triangles, T^V MT].

The global dissociation rate coefficient, k^{Df} , changes with time throughout the relaxation in the chemical reactor, as shown in Fig. 12. This is due to the fact that the state-specific rate coefficients of each rovibrational level differ and the distribution of the molecules in the rovibrational levels changes with time. Only when the system reaches the QSS condition is it possible to define a meaningful global rate coefficient, because the relative populations of the rovibrational levels do not change appreciably. Thus, the value of the plateau in the time evolution of k^{Df} is used to define the QSS reaction rate coefficient, $k_{\text{QSS}}^{\text{Df}}(T)$. This method was first proposed by Bourdon *et al.* [76] for the estimation of the ionization rate coefficient of nitrogen atoms.

At low temperatures, the time required for the establishment of the QSS distribution is shorter than the time before the onset of dissociation. As the temperature increases, the QSS distribution is established only when significant fraction of the molecules has already dissociated. Thus a significant portion of the dissociation occurs at non-QSS conditions when $k^{\text{Df}} < k_{\text{QSS}}^{\text{Df}}(T)$, leading to an overestimation of the rate of dissociation.

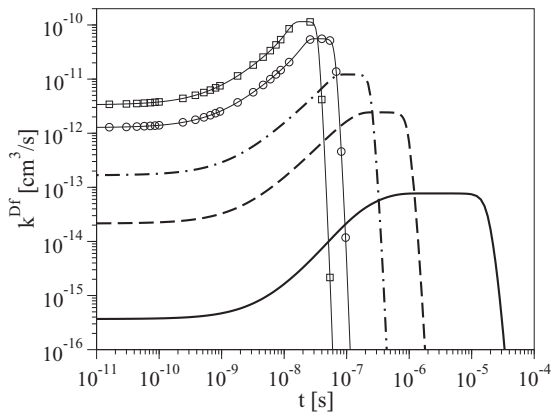


FIG. 12. RVC model. Time evolution of the macroscopic dissociation rate coefficient [33] (unbroken line, $T = 10\,000$ K; dashed line, $T = 15\,000$ K; dotted-dashed line, $T = 20\,000$ K; line with circles, $T = 30\,000$ K; line with squares, $T = 40\,000$ K).

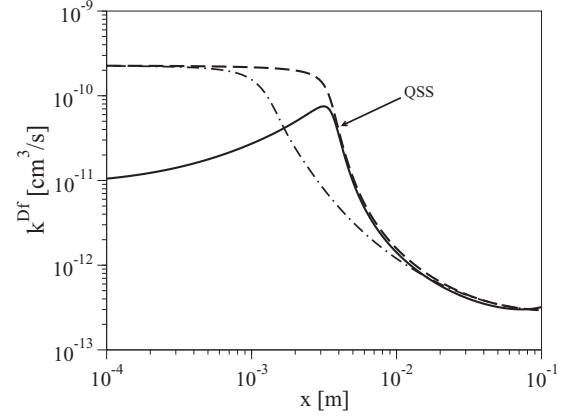


FIG. 13. Estimation of the phenomenological rate coefficient for dissociation k^{Df} in a 0D isothermal reactor, behind the normal shock wave [unbroken line, k^{Df} based on the RVC population distribution and temperature field [Eq. (43)]; dashed line, $k_{\text{QSS}}^{\text{Df}}$ based on the RVC temperature field; and dotted-dashed line, $k_{\text{QSS}}^{\text{Df}}$ based on the MT temperature field].

In the postshock region, the temperature is elevated and the flow residence time is insufficient for the establishment of the QSS distribution. One way to quantify the departure of the nonequilibrium distribution from the QSS distribution is to compare the phenomenological rate coefficient (shown in Fig. 13) with the global instantaneous rate coefficient given by Eq. (43), where the population fractions (n_i/n_{N_2}) are taken from the RVC simulation of the normal shock wave. To facilitate the comparison, we fitted the QSS rate coefficient using a modified Arrhenius form,

$$k_{\text{QSS}}^{\text{Df}}(T) = 1.60 \times 10^{-5} T^{-0.847} \exp(-113\,422/T) \text{ (cm}^3/\text{s)}. \quad (44)$$

Figure 13 compares the instantaneous dissociation rate coefficient k^{Df} given by Eq. (43), for the RVC model, with the one obtained using $k_{\text{QSS}}^{\text{Df}}(T)$ and the translational temperature taken from the RVC model. The early part of the relaxation is characterized by strong deviation from the QSS distribution. $k_{\text{QSS}}^{\text{Df}}(T)$ is about 20 times higher than the actual rate coefficient obtained using the instantaneous $\text{N}_2(1\Sigma_g^+)(i)$ populations. As the relaxation proceeds further, the QSS condition is achieved, and $k_{\text{QSS}}^{\text{Df}}(T) = k^{\text{Df}}$.

The dotted-dashed line in Fig. 13 is the reaction rate constant obtained by using $k_{\text{QSS}}^{\text{Df}}(T)$ with T taken from the MT model, shown in Fig. 1. In the early part of the relaxation, when the dissociation is small and the kinetics is dominated by energy transfer processes, the results also greatly overestimate the dissociation rate and the trend closely reproduces the behavior obtained with the RVC model and the QSS rate coefficient (e.g., dashed line). However, as the relaxation proceeds, the dissociation becomes significant, causing the cooling of the translational temperature and the consequent lowering of the dissociation rate coefficient. In this region the MT and the RVC-QSS curves differ significantly. From this analysis, it is clear that the breakdown of the QSS assumption is responsible for the inability of the MT model to capture the thermal and chemical relaxation directly behind the shock.

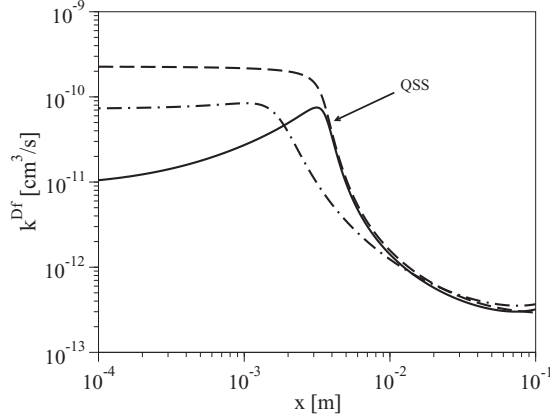


FIG. 14. Estimation of the phenomenological rate coefficient for dissociation k^{Df} , behind the normal shock wave [unbroken line, k^{Df} based on the RVC population distribution and temperature field [Eq. (43)]; dashed line, $k_{\text{QSS}}^{\text{Df}}$ based on the RVC temperature field; and dotted-dashed line, k^{Df} based on the VC population distribution and temperature field].

2. Dissociation dynamics predicted by the VC model

The reasons for the failure of the VC models are investigated next. The starting point is the comparison of the phenomenological dissociation rate coefficient computed with the VC and the RVC models. It is clear, from the analysis of the results shown in Fig. 14, that this model tends to overestimate the dissociation rate [77] in the early part of the relaxation.

To better understand the deficiencies of this model, we need to further characterize the dissociation dynamics of the RVC model. The availability of instantaneous rovibrational population allows us to compute the contribution of each internal level to the dissociation flux. If we divide each of the individual fluxes by the total dissociation flux (i.e., one-way flux),

$$p(E_i) = \frac{k_i^{\text{Df}}(T)n_i}{k^{\text{D}}(T)n_{\text{N}_2}}, \quad (45)$$

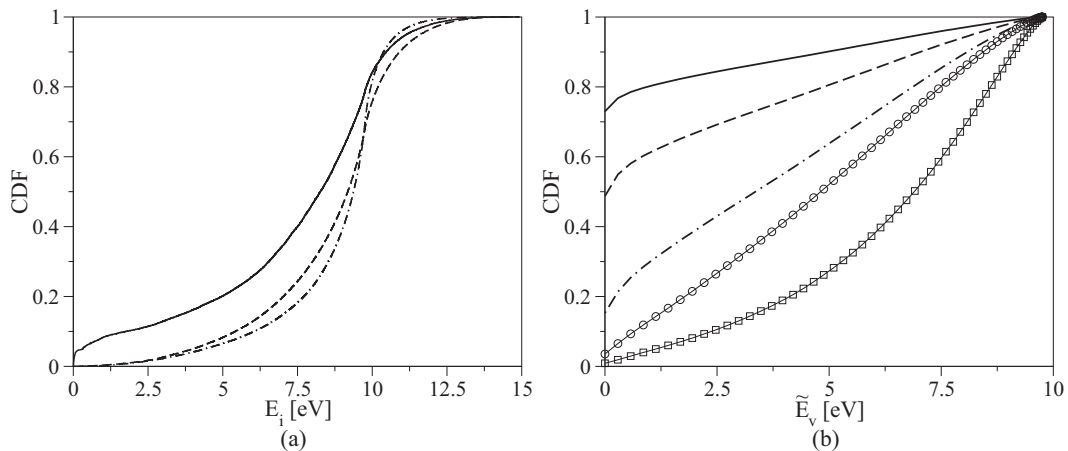


FIG. 15. Cumulative distribution function for the RVC (a) and VC (b) models [in (a) unbroken line, $X_{\text{N}} = 5\%$; dashed line, QSS ($X_{\text{N}} = 50\%$); dotted-dashed line, $X_{\text{N}} = \text{LTE}$; in (b) unbroken line, $X_{\text{N}} = 5\%$; dashed line, $X_{\text{N}} = 10\%$; dotted-dashed line, $X_{\text{N}} = 25\%$; line with circles, $X_{\text{N}} = 50\%$; line with squares, LTE].

we obtain the probability of dissociation from each rovibrational level. Thus, the cumulative distribution function (CDF) is defined as the cumulative sum (or integral in the continuous case) of the probability density function defined above.

In Fig. 15, we have computed the CDF for different locations in the postshock relaxation for the RVC and the VC model. In the case of the RVC model, it is interesting to note that roughly 50% of the dissociation proceeds from the high-lying rovibrational levels (with energies higher than 8 eV). Furthermore, at the onset of the QSS condition, the CDF is “frozen” until the dissociation process approaches the final equilibrium condition. At the equilibrium (LTE) configuration the dissociation is further biased toward the high-lying states.

A similar CDF has been extracted for the VC model. In general, the bulk of the dissociation flux comes from the low-lying vibrational levels. This is not surprising since the predissociated states, which significantly contribute to the dissociation flux in the RVC case, are characterized by low vibrational quantum number. It is clear, from what has been discussed previously, that the assumed equilibrium distribution for the quasibound levels is highly inappropriate and is largely responsible for the overestimation of the dissociation rate. This effect is exacerbated by the assumption of equilibrium between rotation and translational energy modes.

IV. CONCLUSIONS

We have performed an extensive analysis of the nitrogen dissociation in a shock-heated environment. The calculations presented simulate a shock tube experiment with nitrogen molecules being dissociated by collisions with atomic nitrogen in its ground electronic state. The solution of the master equation for the entire rovibrational structure of $\text{N}_2(^1\Sigma_g^+)$, coupled with the one-dimensional Euler flow equations, allowed us to describe accurately the internal energy relaxation and dissociation processes for a wide range of test conditions. The state-to-state approach, adopted in this work, relies on the knowledge of the rovibrational collisional excitation and dissociation rate coefficients, computed as part of the *ab initio*

database developed at the NASA Ames Research Center for the N_2 -N system.

The analysis of the results shows the differences in the dynamics of low-lying, intermediate, and high-lying rovibrationally excited levels. The relaxation of the low-lying vibrational levels can be successfully approximated by a series of Maxwell-Boltzmann distributions for rotational temperature T_v^R , where the temperature of each vibrational level monotonically increases with the vibrational quantum number. The population of the intermediate levels rapidly thermalizes at a common temperature close to the local translational temperature. The dynamics of the quasibound levels drastically differs from the bound levels and it is dominated by their widths. This behavior was already observed by Panesi *et al.* [33] studying the 0D chemical relaxation in an ideal chemical reactor.

We have investigated the influence of spontaneous predissociation and the collisional exchange reaction. While predissociation seems to have a negligible effect on the macroscopic thermodynamic quantities such as temperature and composition, the exchange reaction drastically affects the relaxation by increasing the energy transfer rates and the dissociation.

We have used the rovibrational collisional model to assess the validity of two reduced order models based on simplified kinetics: vibrational collisional and multitemperature models. Both models rely on the same kinetic database used for the rovibrational model. We found that both models are incapable of reproducing the correct chemical and thermal relaxation given by the rovibrational model. The reasons of the disagreement differ depending on the model.

The multitemperature model tends to overestimate the chemical relaxation due to the invalidity of the quasi-steady-state assumption used to derive the phenomenological dissociation rate coefficient. The internal energy relaxation, modeled by using a simple Landau-Teller equations was found to correctly capture the energy transfer process.

The vibrational collisional model tends to overestimate the dissociation rate because of the assumption of equilibrium between rotational and translational energy modes. Furthermore, while the assumption of rotational equilibrium seems to work for the low-lying vibrational levels, the high-lying rotational levels strongly depart from the equilibrium distribution and they tend to be in equilibrium with the free state.

The insights gained by this analysis of nitrogen dissociation serve as guidelines for the development of reduced models. First steps in this direction have already been published by our group [24,54–56].

ACKNOWLEDGMENTS

The authors have benefited from numerous discussions with D. W. Schwenke, G. Chaban, W. Huo, and Y. Liu at the NASA Ames Research Center. We gratefully acknowledge K. Schulz at The University of Texas at Austin for his help in substantially speeding up the code. Funding for this research was provided through a University of Illinois Startup Grant. R.L.J. acknowledges support from NASA's Space Technology/Hypersonics-Entry, Descent and Landing Project and Fundamental Fundamental Aeronautics

Program/Hypersonics Project. A.M. and T.E.M. acknowledge support from the European Research Council Starting Grant No. 259354.

APPENDIX A: VIBRATIONAL DISSOCIATION AND EXCITATION RATE COEFFICIENTS

The vibrational specific rate coefficients for collisional dissociation and excitation are as follows [18]:

$$\tilde{k}_v^{\text{Df}}(T) = \frac{1}{\tilde{Q}_v(T)} \sum_{J \in \mathcal{J}_v} g_{vJ} k_{vJ}^{\text{Df}}(T) \exp\left[-\frac{\Delta \tilde{E}_v(J)}{k_B T}\right], \quad (\text{A1})$$

$$\tilde{k}_{v \rightarrow w}^E(T) = \frac{1}{\tilde{Q}_v(T)} \sum_{J \in \mathcal{J}_v} \sum_{Y \in \mathcal{J}_w} g_{vJ} k_{vJ \rightarrow wY}^E(T) \exp\left[-\frac{\Delta \tilde{E}_v(J)}{k_B T}\right],$$

$$v < w, \quad v, w \in \mathcal{V}. \quad (\text{A2})$$

Rate coefficients for the reverse processes can be obtained based on microreversibility as follows:

$$\frac{\tilde{k}_v^{\text{Df}}(T)}{\tilde{k}_v^{\text{Db}}(T)} = \frac{[g_N Q_N^T(T)]^2}{Q_{N_2}^T(T) \tilde{Q}_v(T)} \exp\left[-\frac{-(2E_N - \tilde{E}_v)}{k_B T}\right], \quad v \in \mathcal{V}, \quad (\text{A3})$$

$$\frac{\tilde{k}_{v \rightarrow w}^E(T)}{\tilde{k}_{w \rightarrow v}^E(T)} = \frac{\tilde{Q}_w(T)}{\tilde{Q}_v(T)} \exp\left[-\frac{-(\tilde{E}_w - \tilde{E}_v)}{k_B T}\right], \quad v < w, \quad v \in \mathcal{V}. \quad (\text{A4})$$

APPENDIX B: ENERGY TRANSFER TERMS

The translational-rotational and translational-vibrational energy transfer terms ($\Omega_{N_2}^{T-R}$ and $\Omega_{N_2}^{T-V}$, respectively) obey a Landau-Teller relaxation model [33],

$$\Omega_{N_2}^{T-R} = n_{N_2} \frac{E_{N_2}^R(T, T) - E_{N_2}^R(T^R, T^V)}{\tau_{N-N_2}^{T-R}(T, p_N)}, \quad (\text{B1})$$

$$\Omega_{N_2}^{T-V} = n_{N_2} \frac{E_{N_2}^V(T, T) - E_{N_2}^V(T^R, T^V)}{\tau_{N-N_2}^{T-V}(T, p_N)}. \quad (\text{B2})$$

The relaxation times $\tau_{N-N_2}^{T-R}$ and $\tau_{N-N_2}^{T-V}$ are functions of the translational temperature \tilde{T} and of the N partial pressure, $p_N = n_N k_B T$. Both relaxation times can be fitted with the following expression:

$$\tau_{N-N_2}^{\text{term}} p_N = \exp[a_0(T^{-1/3} + a_1)] + a_2 \exp[a_3(T^{-1/3} + a_4)]$$

$$(\text{s} \times \text{atm}), \quad (\text{B3})$$

where the a_i fitting coefficients are provided in Table III.

TABLE III. Relaxation time fitting parameters.

Term	a_0	a_1	a_2	a_3	a_4
$T-R$	-60.202	0.26245	-1	-135.875	0.10501
$T-V$	246.747	-0.11930	1	46.9888	-0.41714

The energy transfer terms coupling dissociation with rotational and vibrational energy ($\Omega_{N_2}^{D-R}$ and $\Omega_{N_2}^{D-V}$, respectively) are written by assuming that the average energy lost by N_2 due to dissociation is a temperature-dependent fraction of its dissociation energy [78],

$$\Omega_{N_2}^{D-R} = 2m_N n_{N_2} n_N C_{N_2}^{D-R}(T) 2E_N k_{QSS}^D(T), \quad (\text{B4})$$

$$\Omega_{N_2}^{D-V} = 2m_N n_{N_2} n_N C_{N_2}^{D-V}(T) 2E_N k_{QSS}^D(T). \quad (\text{B5})$$

The dissociation energy fractions for dissociation-rotation and dissociation-vibration coupling ($C_{N_2}^{D-R}$ and $C_{N_2}^{D-V}$,

TABLE IV. Dissociation energy fraction fitting parameters.

Term	b_0	b_1
$D-R$	-0.99138	0.13029
$D-V$	5.867	-0.23341

respectively) can be fitted with the following relations:

$$C_{N_2}^{D-R} = b_0 + b_1 \ln(T), \quad (\text{B6})$$

$$C_{N_2}^{D-V} = b_0 T^{b_1}, \quad (\text{B7})$$

where the b_i fitting coefficients are provided in Table IV.

-
- [1] P. A. Gnoffo, *Annu. Rev. Fluid Mech.* **31**, 459 (1999).
- [2] C. Park, *Nonequilibrium Hypersonic Aerothermodynamics* (John Wiley & Sons, New York, 1989).
- [3] D. Giordano, *Non-Equilibrium Gas Dynamics from Physical Models to Hypersonic Flights*, AVT-162 RTO AVT/VKI Lecture Series held at the von Karman Institute, Rhode St. Genese, Belgium, 8–12 September 2008. Published in September 2009, RTO-EN-AVT-162.
- [4] G. V. Candler and R. MacCormack, *J. Thermophys. Heat Tr.* **5**, 266 (1991).
- [5] S. Chapman and T. Cowling, *The Mathematical Theory of Non-Uniform Gases* (Cambridge University Press, London, 1970).
- [6] V. Giovangigli, *Multicomponent Flow Modeling* (Birkhäuser, Berlin, 1999).
- [7] R. Brun, *Introduction à la Dynamique des Gaz Réactifs* (Cepadues Editions, Toulouse, 2006).
- [8] E. Nagnibeda and E. Kustova, *Non-Equilibrium Reacting Gas Flows* (Springer-Verlag, Berlin, 2009).
- [9] F. Thivet, M. Y. Perrin, and S. Candel, *Phys. Fluids* **3**, 2799 (1991).
- [10] B. Graille, T. Magin, and M. Massot, *Math. Models Methods Appl. Sci.* **19**, 527 (2009).
- [11] T. E. B. Magin and G. Degrez, *Phys. Rev. E* **70**, 046412 (2004).
- [12] E. V. Kustova and L. A. Puzyreva, *Phys. Rev. E* **80**, 046407 (2009).
- [13] M. Capitelli, R. Celiberto, C. Gorse, A. Laricchiuta, D. Pagano, and P. Traversa, *Phys. Rev. E* **69**, 026412 (2004).
- [14] D. Bose and G. Candler, *J. Chem. Phys.* **104**, 2825 (1996).
- [15] D. Bose and G. Candler, *J. Chem. Phys.* **107**, 6136 (1997).
- [16] A. Bourdon, M. Panesi, A. Brandis, T. Magin, G. Chaban, W. Huo, R. Jaffe, and D. W. Schwenke, in *Proceedings of the 2008 Summer Program – Center for Turbulence Research, Stanford University, Palo Alto, California, July 2008*, pp. 5–16.
- [17] M. Panesi, E. T. Magin, A. Munafò, A. Bourdon, R. L. Jaffe, and D. W. Schwenke, in *Proceedings of the 2010 Summer Program – Center for Turbulence Research, Stanford University, Palo Alto, California, July 2010*, pp. 445–454.
- [18] A. Munafò, M. Panesi, R. L. Jaffe, G. Colonna, A. Bourdon, and T. E. Magin, *Eur. Phys. J. D* **66**, 188 (2012).
- [19] M. Capitelli, G. Colonna, and F. Esposito, *J. Phys. Chem. A* **108**, 8930 (2004).
- [20] J. Kim and I. Boyd, *Chem. Phys.* **415**, 237 (2013).
- [21] F. Esposito, I. Armenise, and M. Capitelli, *Chem. Phys.* **331**, 1 (2006).
- [22] B. Gordiets, A. I. Osipov, E. V. Stupochenko, and L. A. Shelepin, *Sov. Phys. Usp.* **15**, 759 (1973).
- [23] M. Panesi, T. E. Magin, A. Bourdon, A. Bultel, and O. Chazot, *J. Thermophys. Heat Tr.* **23**, 236 (2009).
- [24] M. Panesi, T. E. Magin, A. Bourdon, A. Bultel, and O. Chazot, *J. Thermophys. Heat Tr.* **25**, 361 (2011).
- [25] C. O. Laux, L. Pierrot, and R. J. Gessman, *Chem. Phys.* **398**, 46 (2012).
- [26] G. Billing and E. Fisher, *Chem. Phys.* **43**, 395 (1979).
- [27] E. Josyula and W. Bailey, *J. Thermophys. Heat Tr.* **15**, 157 (2001).
- [28] E. Josyula, W. Bailey, and S. Ruffin, *Phys. Fluids* **15**, 3223 (2003).
- [29] G. Colonna, M. Tuttafesta, M. Capitelli, and D. Giordano, *J. Thermophys. Heat Tr.* **13**, 372 (1999).
- [30] G. Colonna and M. Capitelli, *J. Thermophys. Heat Tr.* **15**, 308 (2001).
- [31] G. Colonna, I. Armenise, D. Bruno, and M. Capitelli, *J. Thermophys. Heat Tr.* **20**, 477 (2006).
- [32] I. Armenise, M. Capitelli, R. Celiberto, G. Colonna, C. Gorse, and A. Lagana, *Chem. Phys. Lett.* **227**, 157 (1994).
- [33] M. Panesi, R. L. Jaffe, D. Schwenke, and E. T. Magin, *J. Chem. Phys.* **138**, 044312 (2013).
- [34] K. Haug, D. Truhlar, and N. Blais, *J. Chem. Phys.* **86**, 2697 (1987).
- [35] D. W. Schwenke, *J. Chem. Phys.* **92**, 7267 (1990).
- [36] J. Kim and I. Boyd, *Phys. Fluids* **24**, 086102 (2012).
- [37] I. V. Adamovich and J. W. Rich, *J. Chem. Phys.* **109**, 7711 (1998).
- [38] S. O. Macheret and I. V. Adamovich, *Chem. Phys.* **17**, 113 (2000).
- [39] D. A. Gonzales and P. L. Varghese, *J. Phys. Chem.* **97**, 7612 (1993).
- [40] D. A. Gonzales and P. L. Varghese, *J. Thermophys. Heat Tr.* **8**, 237 (1994).

- [41] D. A. Gonzales and P. L. Varghese, *Chem. Phys.* **195**, 83 (1995).
- [42] A. Aliat, A. Chikhaoui, and E. V. Kustova, *Phys. Rev. E* **68**, 056306 (2003).
- [43] A. Aliat, P. Vedula, and E. Josyula, *Phys. Rev. E* **83**, 026308 (2011).
- [44] A. Aliat, P. Vedula, and E. Josyula, *Phys. Rev. E* **83**, 037301 (2011).
- [45] A. Aliat, P. Vedula, and E. Josyula, *Phys. Rev. E* **83**, 067302 (2011).
- [46] I. Boyd, *Phys. Fluids* **2**, 447 (1990).
- [47] I. Boyd, *Phys. Fluids* **5**, 2278 (1993).
- [48] I. J. Wysong and D. C. Wadsworth, *Phys. Fluids* **10**, 2983 (1998).
- [49] C. Park, *J. Thermophys. Heat Tr.* **18**, 527 (2004).
- [50] K. Fujita, *48th AIAA Aerospace Sciences Meeting Including the New Horizons Forum and Aerospace Exposition, 4–7 January 2010, Orlando, Florida*, AIAA 2010-1568 (2010).
- [51] R. N. Schwartz, Z. I. Slawsky, and K. F. Herzfeld, *J. Chem. Phys.* **20**, 1591 (1952).
- [52] M. L. Da Silva, V. Guerra, and J. Loureiro, *J. Thermophys. Heat Tr.* **21**, 303 (2007).
- [53] A. Guy, A. Bourdon, and M.-Y. Perrin, *Chem. Phys.* **420**, 15 (2013).
- [54] M. Panesi and A. Lani, *Phys. Fluids* **25**, 057101 (2013).
- [55] T. E. Magin, M. Panesi, A. Bourdon, R. L. Jaffe, and D. W. Schwenke, *Chem. Phys.* **398**, 90 (2012).
- [56] A. Munafò, M. Panesi, and T. E. Magin, *Phys. Rev. E* **89**, 023001 (2014).
- [57] R. L. Jaffe, D. W. Schwenke, G. Chaban, and W. Huo, *Proceedings of the 46th AIAA Aerospace Sciences Meeting and Exhibit, Reno*, AIAA paper 2008-1208 (AIAA, Reston, VA, 2008).
- [58] G. Chaban, R. L. Jaffe, D. W. Schwenke, and W. Huo, in *Proceedings of the 46th AIAA Aerospace Sciences Meeting and Exhibit, Reno*, AIAA paper 2008-1209 (2008).
- [59] D. W. Schwenke, VKI LS 2008, *Non-equilibrium Gas Dynamics, Rhode-Saint-Genèse, Belgium, 8–12 Sept. 2008*, AIAA paper AVT-162 RTO AVT/VKI (2008).
- [60] R. L. Jaffe, D. W. Schwenke, and C. Chaban, in *Proceedings of the 47th AIAA Aerospace Sciences Meeting Including the New Horizons Forum and Aerospace Exposition, Orlando*, AIAA paper 2009-1569 (AIAA, Reston, VA, 2009).
- [61] R. L. Jaffe, D. W. Schwenke, and G. Chaban, in *10th AIAA/ASME Joint Thermophysics and Heat Transfer Conference, 28 June–1 July 2010, Chicago, Illinois*, AIAA-2010-4517 (2010).
- [62] M. Panesi, R. L. Jaffe, and D. W. Schwenke, *Fluid Dynamics and Co-located Conferences June 24–27, 2013, San Diego, CA*, AIAA Paper 2013–3147 (2013).
- [63] R. L. Jaffe, *22nd AIAA Thermophysics Conference, Honolulu, Hawaii*, AIAA Paper 1987–1633 (1987).
- [64] D. W. Schwenke, *J. Chem. Phys.* **89**, 2076 (1988).
- [65] R. Le Roy, Y. Huang, and C. Jary, *J. Chem. Phys.* **125**, 164310 (2006).
- [66] E. Nagnibeda and E. Kustova, *Non-Equilibrium Reacting Gas Flows* (Springer, Berlin, 2009).
- [67] K. Radhakrishnan and A. C. Hindmarsh, NASA Report 1327 (1993).
- [68] F. Esposito, M. Capitelli, and C. Gorse, *Chem. Phys.* **257**, 193 (2000).
- [69] D. Olynick and H. Hassan, *J. Thermophys. Heat Tr.* **7**, 687 (1993).
- [70] T. Holman and I. Boyd, *J. Thermophys. Heat Tr.* **23**, 660 (2009).
- [71] T. Deschenes, T. Holman, and I. Boyd, *J. Thermophys. Heat Tr.* **25**, 218 (2011).
- [72] J. G. Parker, *Phys. Fluids* **2**, 449 (1959).
- [73] C. Guldberg, *Forhandling i Videnskabs-Selskabet i Christiania*, 111 (1864).
- [74] P. Waage, *Forhandling i Videnskabs-Selskabet i Christiania*, 92 (1864).
- [75] C. Park, *AIAA* **7**, 1653 (1969).
- [76] A. Bourdon and P. Vervisch, *Phys. Rev. E* **54**, 1888 (1996).
- [77] $k^{\text{Df}} = (1/n_{\text{N}_2}) \sum_{v \in \mathcal{V}} \tilde{n}_v \tilde{k}_v^{\text{Df}}(T)$.
- [78] This model is similar to the one proposed by Park [2] where the average vibrational energy lost by a molecule due to dissociation is 30% of its dissociation energy.